AIAA SciTech Forum
9 - 13 January 2017, Grapevine, Texas
55th AIAA Aerospace Sciences Meeting

Application of Detached Eddy Simulation to a Bluff Body Flame Stabilizer in Duct Flow

Jonathan P. West * and Clinton P. T. Groth †
University of Toronto Institute for Aerospace Studies,
4925 Dufferin St., Toronto, Ontario, M3H 5T6, Canada

John T. C. Hu ‡
Pratt & Whitney Canada
1801 Courtneypark Dr., Mississauga, Ontario, L5T 1J3, Canada

Detached eddy simulation (DES) is a hybrid turbulence model that makes use of both Reynolds-averaged Navier-Stokes (RANS) and large eddy simulation (LES) strategies depending on the mesh resolution. It is one of the more successful hybrid RANS/LES methods and is thought to have significant potential for the prediction of turbulent reactive flows. In the present study, the application of DES to the prediction of a turbulent reactive flow associated with a bluff body flame stabilizer in a duct flow is examined. This bluff body stabilizer configuration consists of a triangular obstruction in a planar duct and involves a turbulent premixed propane-air flame. It has been studied previously and experimental data exists for both non-reacting and reacting flow operation. A mesh study and boundary condition parameter study was first considered for the non-reacting flow case. A similar mesh study was also performed for the reactive case. The predictive performance of DES for the non-reacting case was also compared to those of the standalone unsteady RANS (URANS) model, standalone LES models, as well as results obtained assuming laminar flow. For the non-reacting case, it is shown that at least two different unsteady solution modes associated with unsteady vortex shedding from the bluff body are possible in the numerical solutions, depending on the specification of the inlet pressure and initial conditions. Smaller differences are observed in the cold-flow DES simulation results for the range of mesh resolutions studied, indicating that grid convergence is approached for both mean and RMS flow quantities. For the reactive flow case, an algebraic flamelet model requiring the solution of an averaged/filtered progress variable was used to model turbulence/chemistry interaction. For this case, several features of the flame structure observed in the experiments were not well reproduced in the DES results and, unlike the non-reacting case, mesh independence was not observed far downstream of the stabilizer. Some of the discrepancies are thought to be associated with the rather simplified flamelet combutstion model adopted herein.

I. Introduction

Turbulence is a continuum phenomenon, the physics of which is captured by the Navier-Stokes equations without modelling. Simulating turbulent flows with the Navier-Stokes equations without the aid of a model would be ideal; practically however, it is too expensive computationally to resolve the Navier-Stokes equations over the full range of turbulent scales for engineering problems. As a consequence, simulations of practical engineering problems require that the turbulence must be modelled to some degree. Reynolds-averaged Navier-Stokes (RANS) methods provide a low computational cost and good near-wall modelling but must

*Ph.D. Candidate, Email: j.west@mail.utoronto.ca, and AIAA Student Member.
†Professor, Email: groth@utias.utoronto.ca , and AIAA Senior Member.
‡Manager, Hot Section Technology, Email: john.hu@pwc.ca.

model the full range of turbulent scales without resolving even large scale turbulent features. As a result, they often fail to properly capture information about unsteady flow features and turbulent mixing. Large eddy simulation (LES) methods only model turbulent structures on the smallest scales and resolve the remaining scales without modelling. However, LES methods can in many instances be computationally too expensive near walls for practical three-dimensional geometries unless paired with an empirical wall model, which is generally considered less sophisticated than a RANS model near walls as discussed by Fröhlich *et al.*[1]

Detached eddy simulation (DES), as a hybrid RANS/LES method, can potentially circumvent some of the weaknesses of standalone RANS and LES models by using LES outside of boundary layers and reserving RANS only for near-wall and/or under resolved regions. DES is a very popular type of hybrid RANS/LES model and has been widely applied for non-reacting flows[2–4] , further studies are also discussed in a review by Spalart[5]. DES has also been applied to reacting flows in previous studies by Choi *et al.*[6] and Sainte-Rose *et al.*[7,8] and may have significant potential for predicting turbulent reactive flows. Nevertheless, the application of DES to reactive flow simulation, particularly for practical combustor conditions, requires further study.

II. Scope of Study

In the present research, the application of DES to the prediction of turbulent reactive flow associated with a bluff body flame stabilizer in a duct flow is investigated. The specific DES model utilized in this study was derived from the Shear Stress Transport (SST) k-ω RANS model of Menter *et al.*[9]. A rather simple algebraic flamelet model requiring the solution of an averaged/filtered progress variable is used to model turbulence/chemistry interaction in the simulations. The burner configuration examined in this study, the bluff body flame stabilizer in a duct flow of Sjunnesson *et al.*[10,11], utilizes a triangular obstruction in a duct as a flame holder and involves a premixed propane-air flame. This benchmark case is associated with complex unsteady flow features and both non-reacting and reacting flow experimental data is available for comparison to numerical predictions. The unsteadiness of this burner configuration is attributable to unsteady vortex shedding behaviour in the non-reacting flow case as described in Sjunnesson *et al.*[10] and combustion induced pressure oscillations and shear layer roll-up in the reactive flow case as described in in Sjunnesson *et al.*[10,11]. For these reasons, the bluff body stabilizer has been frequently studied by multiple authors to investigate the performance of LES turbulence models[12–15], several hybrid RANS/LES models[16,17], as well as DES models[18,19]. It is also the focus of the 2017 Model Validation for Propulsion (MVP) workshop.[20]

For comparative purposes, the DES simulations of the non-reactive flow case are compared to those of the standalone unsteady RANS (URANS) model, two standalone LES models, as well as results obtained assuming laminar flow. For the reactive case, only DES results are reported. The commercial code Ansys FLUENT was used to perform all of the simulations herein, as it includes implementations for all of the turbulence modelling approaches along with the premixed combustion model utilized in this study. This allowed for comparisons using the same meshes with minimal change in the underlying numerical method. The specific alternative turbulence treatments considered here are as follows:

- URANS model: SST k-ω model of Menter *et al.*[9];
- LES model: Smagorinsky-Lilly model as described in Piomelli *et al.*[21] with wall modelling; and
- dynamic LES (DLES) model: variant of the Smagorinsky-Lilly model with dynamic evaluation of the subfilter scale turbulent viscosity as described in Germano *et al.*[22] with wall modelling.

Within Ansys FLUENT, the SIMPLE finite-volume solution algorithm of Patankar *et al.* [23] was utilized for dealing with the pressure-velocity coupling and the second-order upwind scheme of Barth *et al.* [24] was applied for pressure interpolation. Time advancement was accomplished using a second-order accurate dual-time-stepping approach in which sub-iterations at each time step were used to converge the solution for the temporally discretized equations.

To investigate the mesh sensitivity of the bluff-body flame stabilizer solution, a mesh study utilizing three structured meshes with varying resolution was conducted for both cold and hot flows. For the non-reacting case, the results of the mesh study inspired a boundary condition sensitivity study that informed subsequent solution parameter choices for the simulations.

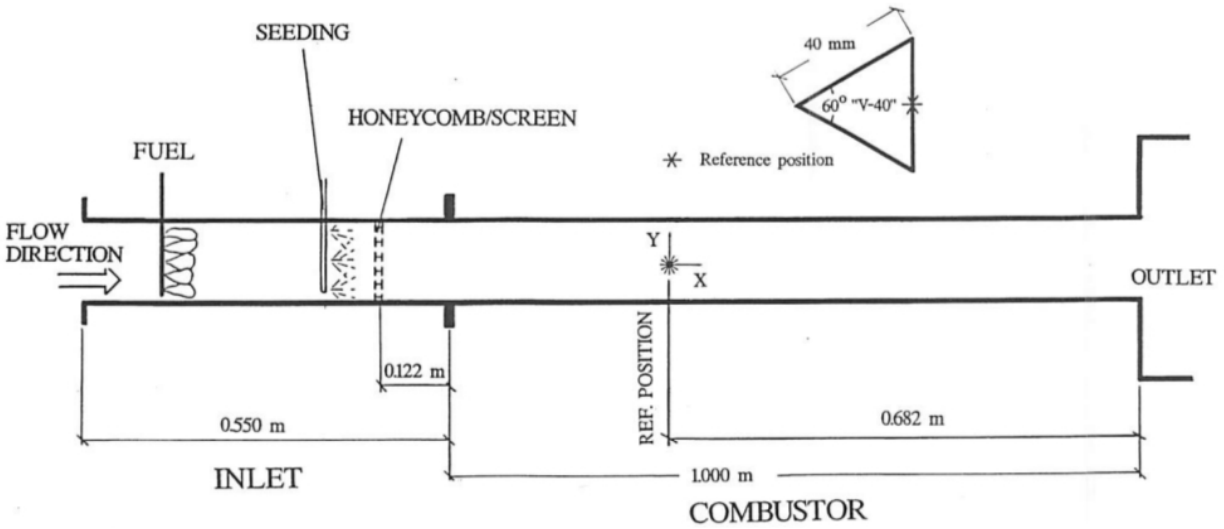

Figure 1. Schematic diagram of bluff body flame stabilizer in duct burner configuration of Sjunnesson *et al.*[10]

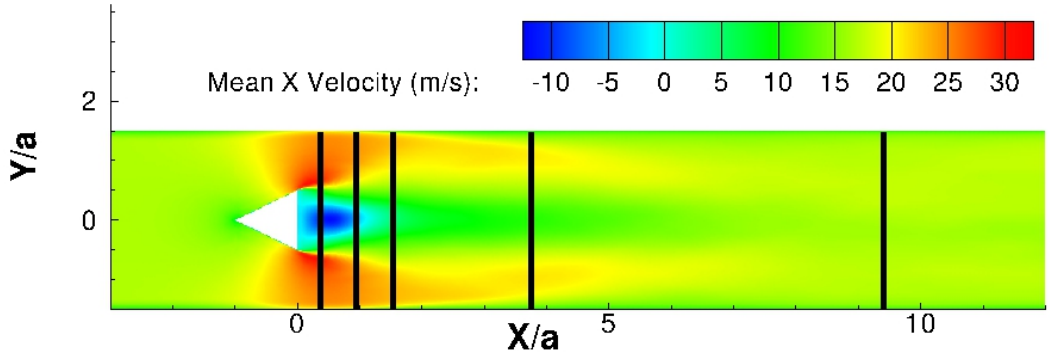

Figure 2. Locations of the profile stations (black) for comparisons of numerical and experimental results as shown on the predicted distributions of the mean axial velocity distribution for the non-reactive flow field of the bluff body flame stabilizer in duct case.

III. Bluff Body Flame Stabilizer in Duct Flow

The bluff body flame stabilizer in duct flow case of Sjunnesson *et al.*[10] utilizes an triangular obstruction with equal edge lengths of 0.04 m in a duct flow with a cross section of 0.12 m by 0.24 m as an analogy to a flame holder. As mentioned, both reacting and non-reacting experiments were conducted. The apparatus is composed of an inlet section 0.55 m in length and a combustor section that is 1 m in length. The inlet section contains fuel injectors for the reacting case and flow particle seeding devices for laser Doppler anemometry (LDA) measurements prior to honeycomb screens. The combustor section is simply a duct with the triangular obstruction centred along the 0.12 m dimension and spanning the 0.24 m dimension oriented with the downstream face perpendicular to the flow. The perpendicular face is located 0.318 m downstream from the beginning of the combustor section. The apparatus is shown in Figure 1.

For the non-reacting case, air with a bulk velocity of 16.6 m/s flowed through the apparatus. For the reacting case, a premixed propane-air mixture with a equivalence ratio of 0.65 and a bulk velocity of 17.3 m/s flowed into the apparatus. Both the non-reacting and reacting flows entered at a temperature of 288 K. The measured turbulence intensity past the honeycomb screens was between 3% and 4%. The flow Reynolds number based on the edge length of the obstruction was 45 000 for the non-reacting case and 47 000 for the reacting case. The mean and root-mean-square (RMS) velocity at stations downstream of the obstruction were obtained by Sjunnesson *et al.*[10] using LDA measurements. These values were extracted directly from the published results[10] for comparison to the present simulations. Coherent anti-stokes Raman scattering (CARS) was also used by Sjunnesson *et al.*[10,11] to collect measurements of the temperature of the reactive

flow field, which is also compared to the present DES predictions.

Note that for all comparisons presented herein, distances were non-dimensionalized with respect to the width of the bluff body, a, which is 0.04 m. Furthermore, the numerical and experimental results for this case were primarily compared at velocity profile stations located down stream of the bluff body across the span of the duct as shown in Figure 2.

IV. Premixed Flame Combustion Model

For the premixed propane-air flame of interest here, the combustion model utilized is a premixed flamelet-type c-equation model as discussed in the textbook of Poinsot and Veynante[25] as well as the works of Bray[26] and Zimont,[27] where c is a progress variable that is technically defined as

$$c = \frac{\sum_{i=1}^{n} Y_i}{\sum_{i=1}^{n} Y_{i,eq}} \tag{1}$$

and where Y_i is the current mass fraction of a product species i and $Y_{i,eq}$ is the equilibrium (fully burnt) mass fraction of a product species i. As such, c has values of 0 for an un-burnt mixture and 1 for a burnt mixture.

In this relatively simple flamelet model, the combustion is related to the advancement of a flame front and it is assumed that the advancing thin flame sheet converts un-burnt reactants into burnt reactants. This flame front is also distorted by the turbulence. It therefore follows that the combustion model is strongly connected to the turbulence model. As such, a mean progress variable, $\overline{c}$, is tracked in this premixed combustion model instead of an instantaneous value. The transport equation for $\overline{c}$ is assumed to have the form

$$\frac{\partial}{\partial t}\left(\rho\overline{c}\right) + \frac{\partial}{\partial x_i}\left(\rho U_i \overline{c}\right) = \frac{\partial}{\partial x_j}\left(\frac{\mu_t}{\mathrm{Sc_t}}\frac{\partial \overline{c}}{\partial x_j}\right) + G\rho S_c \tag{2}$$

where μ_t is the turbulent viscosity, $\mathrm{Sc_t}$ is the turbulent Schmidt number which is by default defined as 0.7, ρS_c is the source term that is used to model the combustion process of the flame front, and G is a flame stretch factor meant to model the probability that stretching will not quench the fame.

The source term, S_c, appearing in Equation (2) is defined as

$$\rho S_c = \rho_u U_t \left|\frac{\partial \overline{c}}{\partial x_i}\right| \tag{3}$$

where ρ_u is the un-burnt mixture density and U_t is the turbulent flame speed. The turbulent flame speed is calculated here using the Zimont model.[27] In the Zimont model, U_t is calculated as

$$U_t = A(u')^{3/4} U_l^{1/2} \alpha^{-1/4} l_t^{1/4} \tag{4}$$

where A is a model constant equal to 0.52, u' is the root mean square velocity, U_l is the laminar flame speed, α is the molecular heat transfer coefficient for the un-burnt mixture, and l_t is the turbulent length scale. Values of U_l and α are properties of the un-burnt mixture. For the propane-air mixture of interest here, U_l is take to have a value of 0.17 m/s and α is set to 2×10^{-5} m^2/s. The root mean square speed, u', is calculated from the turbulent kinetic energy, k, and also used in the calculation of l_t

$$l_t = C_D \frac{(u')^3}{\varepsilon} \tag{5}$$

where C_D is a constant equal to 0.37 and ε is the dissipation rate of k.

The flame stretch factor G utilized in Equation (2) is defined as

$$G = \frac{1}{2}\mathrm{erfc}\left[-\sqrt{\frac{1}{2\sigma}}\left(\ln\frac{\varepsilon_{\mathrm{cr}}}{\varepsilon} + \frac{\sigma}{2}\right)\right] \tag{6}$$

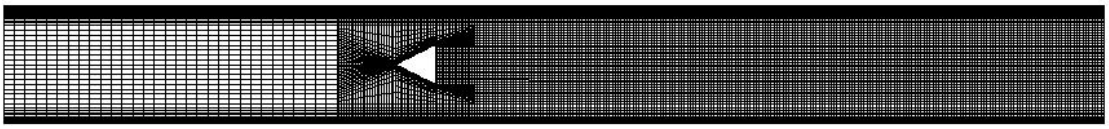

(a) Coarse mesh (872 326 cells).

(b) Medium mesh (1 752 840 cells).

(c) Fine mesh (3 513 963 cells).

Figure 3. Coarse, medium, and fine meshes used in bluff body flame stabilizer in duct flow simulations.

where σ is defined as the standard deviation of the turbulent kinetic energy dissipation rate, ε, and calculated as

$$\sigma = \mu_{str} \ln\left[\frac{\ell}{\eta}\right] \tag{7}$$

and ε_{cr} is the critical dissipation rate and calculated as

$$\varepsilon_{cr} = 15 v g_{cr}^2 \tag{8}$$

where μ_{str} is a model constant set to 0.26, ℓ is the integral length scale, η is the Kolmogorov scale, and g_{cr} is the critical rate of strain. Zimont *et al.*[27] suggested values for the critical rate of strain, g_{cr}, are in the range of $3\ 000 \leq g_{cr} \leq 8\ 000\ \text{s}^{-1}$; however, this parameter should probably be tuned for the specific case. As such, a parameter study of g_{cr} was beyond the scope of the present study. This local extinction model was therefore turned off by setting g_{cr} to an arbitrarily high value of $1 \times 10^8\ \text{s}^{-1}$. Nevertheless, tuning of g_{cr} would seem preferable and should be considered in future follow-on studies.

In the c-equation model, the flow temperature is taken to be a function of $\bar{c}$. Values for the temperature are linearly interpolated in terms of the progress variable between 288 K, representing the temperature of the un-burnt gases, and the adiabatic flame temperature of 1784 K for the propane fuel, representing the temperature of the fully burnt reactants.

V. Computational Domain and Mesh Design

For the numerical results presented herein, three structured meshes of varying resolution were considered in which the overall number of cells from one mesh to the next was increased by a factor of approximately

Table 1. Computational meshes used in simulation of bluff body flame stabilizer in duct flow.

Mesh	Number of Cells	Cell Width (m) Downstream of Bluff Body
Coarse	872 326	∼0.0024
Medium	1 752 840	∼0.0019
Fine	3 513 963	∼0.0015
MVP workshop 4 mm	809 080	∼0.004
MVP workshop 2 mm	2 613 440	∼0.002
MVP workshop 1 mm	11 331 200	∼0.001

(a) 4 mm MVP workshop mesh (809 080 cells).

(b) 2 mm MVP workshop mesh (2 613 440 cells).

(c) 1 mm MVP workshop mesh (11 331 200 cells).

Figure 4. Coarse, medium, and fine meshes proposed for bluff body flame stabilizer in duct flow simulations by MVP workshop organizers.

two. The mesh naming scheme and size of the meshes are summarized in Table 1. A coarse mesh containing 872 326 computational cells represented the coarsest resolution considered and medium and fine meshes consisting of 1 752 840 and 3 513 963 cells, respectively, were also used. The general structure and layout of the coarse, medium, and fine meshes are shown in Figure 3. It should be noted that, three meshes were made available by the MVP Workshop[20] for simulating the bluff-body flame stabilizer flow, namely a coarse 4 mm mesh, a medium 2 mm mesh, and a fine 1 mm mesh which are additionally shown in Figure 4 for comparison purposes. The statistics of the workshop meshes are also summarized in Table 1. The workshop meshes were not used for the numerical simulation herein (these meshes will be examined in future follow-on studies), it should be pointed out that the medium mesh used in the current study has a similar resolution to that of the 2 mm workshop mesh whereas the 4 mm workshop mesh is slightly coarser than the coarse mesh considered here and the fine 1 mm workshop has a slightly higher resolution than that of the fine mesh used here. Note also that the upstream portion of the computational coarse, medium, and fine meshes ahead of the stabilizer is slightly longer than the corresponding length used in the workshop meshes, with the upstream region extending from the honeycomb screens to the obstruction. For completeness, the distribution of mesh size with the computational domain is depicted in Figure 5 for the coarse, medium, and fine meshes.

As noted above, in the current simulations, the duct inlet was placed 0.44 m upstream of the downstream side of the triangular obstruction, where the honeycomb screens were in the experimental apparatus. The duct outlet was placed 0.682 m downstream of the triangular obstruction which is consistent with the experimental apparatus. The bottom and top walls are placed 0.12 m apart as is consistent with the experimental apparatus. To save on computational costs the transverse boundaries of the domain were taken to be periodic boundaries set 0.08 m apart. A similar strategy was used by Cocks *et al.*[12]. The intended benefit afforded by the DES method considered herein was to save on computational costs by remaining in URANS mode upstream of the bluff body and switching to LES mode in the vicinity and downstream of the obstruction. Based on the recommendations of Spalart,[28] this was accomplished in the DES simulations by utilizing a zonal meshing strategy. Therefore, the region of the duct from the inlet to the LES region was meshed somewhat coarsely, but with high aspect ratio near the duct walls to allow RANS integration to the wall. The mesh transition to a LES region was started 0.06 m upstream of the leading edge of the obstruction to ensure LES treatment of any vortex shedding phenomenon. In this region cells were meshed in accordance with the cell widths specified in Table 1 and with largely isotropic cells. However, computational cells in the near wall on the upstream faces of the bluff body were clustered to allow some degree of RANS integration to the wall.

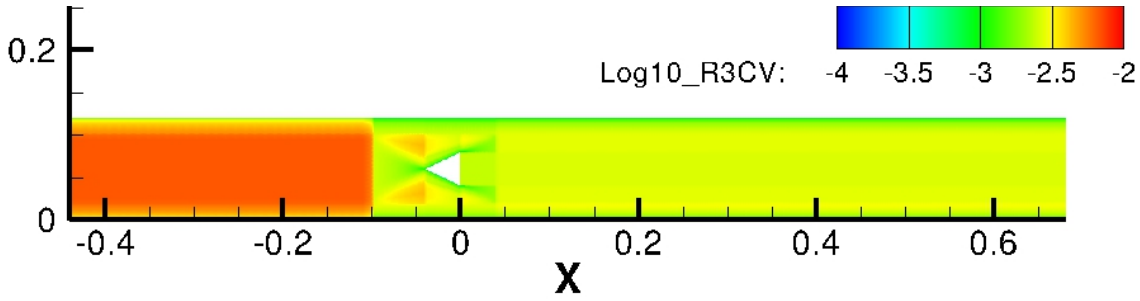

(a) Contours of Log10 of cubic root of cell volume for coarse mesh.

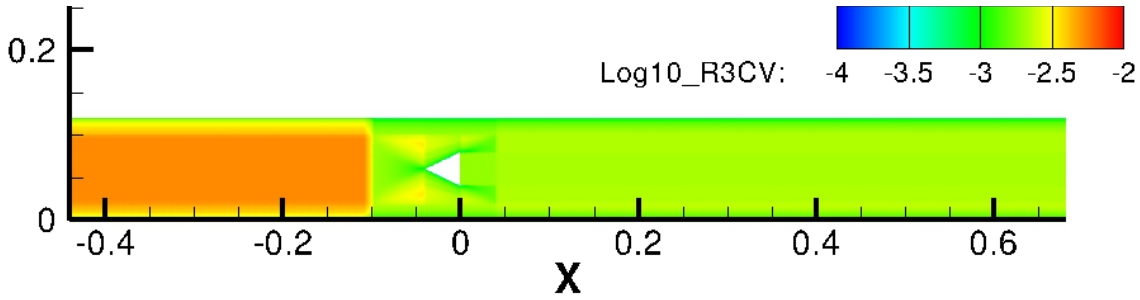

(b) Contours of Log10 of cubic root of cell volume for medium mesh.

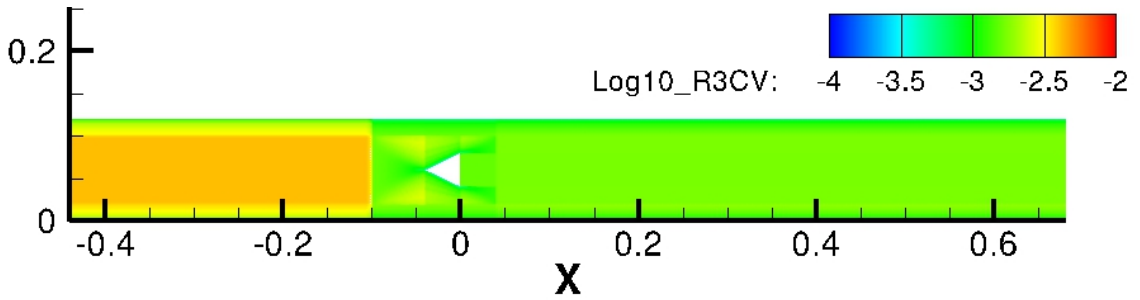

(c) Contours of Log10 of cubic root of cell volume for fine mesh.

Figure 5. Computational mesh size for coarse, medium, and fine meshes used in bluff body flame stabilizer in duct flow simulations.

It should also be mentioned that, for the reacting cases, the combustion model was limited to the area past the bluff body obstruction and 2 mm offset from the duct walls. This was accomplished by adjusting the progress variable, $\bar{c}$, to zero outside the reaction zone at each iteration. As mentioned above, the local extinction model was not utilized. Without modelling local extinction, this limiting operation was necessary to prevent the non-physical progression of the premixed flame upstream along the walls of the duct and stabilizer.

VI. DES Results and Discussion for Non-Reactive Flow Field

The non-reacting case of the bluff-body flame stabilizer in duct flow of Sjunnesson *et al.*[10] is first studied in order to evaluate the ability of DES to predict the turbulence and unsteady features associated with this burner in isolation from the combustion model. The associated mesh study spurred a follow-on study of the influence that boundary data and initialization conditions have on the DES results for this case. Taking into account the insights gained from the mesh and parameter studies of boundary and initial data specification, the DES predictions are then compared to alternative turbulence treatment strategies such as URANS, LES, and DLES.

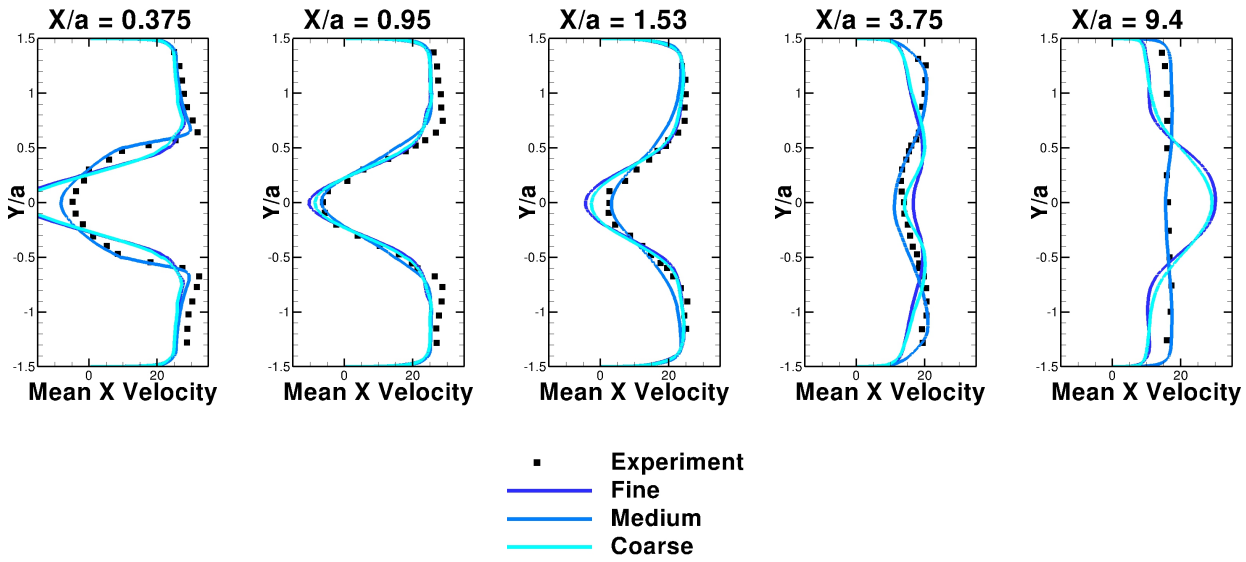

Figure 6. Non reacting bluff body flame stabilizer in duct flow initial mesh study mean axial velocity (m/s).

VI.A. Results of Mesh and Boundary Condition Parameter Studies

The DES results were first obtained on the three meshes with successively increasing resolution as summarized in Table 1 using the following procedure:

- the computational domain was set up with a velocity inlet corresponding to the experimental value of 16.6 m/s[10] and a pressure outlet;
- a preliminary steady RANS prediction was then obtained in order to provide an initial flow field for the DES computations (due to the vortex shedding, the RANS simulations did not fully converge to a steady state solution but the results were considered to be more reasonable than applying a uniform constant velocity every where);
- the DES computations on each mesh was then initialized with the corresponding RANS flow field and the DES simulations were then carried out for a time period of $T = 0.375s \sim 5\,(L/U_{inlet})$ prior to the collection of the flow field statistics; and
- Each DES computation was then continued for $T = 0.375s \sim 5\,(L/U_{inlet})$ to collect flow statistics which are then reported below.

Interestingly as depicted in Figures 6 and 7, the resulting DES predictions of the mean and RMS axial velocity profiles obtained on the medium mesh with the above procedure showed correct adherence to the experimental results while the DES results for the fine and coarse meshes were in agreement with each other but were not in agreement with the experimental results.

Additionally, it is evident from the centerline pressure profiles of the DES solutions starting at the inlet boundary, as given in Figure 8, that the fine and coarse mesh solutions were operating at significantly different inlet pressures in order to maintain the same inlet velocity suggesting that the flow physics occurring in the fine and coarse mesh simulations was significantly different from the medium mesh simulation. It is also evident that the vortices for the cases that obtained incorrect solutions were stronger and more coherent as shown in a comparison of fine and medium mesh instantaneous spanwise vorticity contours in Figures 9 and 10. Due to the differences in these vortices there were also significant differences between the average axial velocities of the fine and medium mesh solutions as shown in Figure 11. These results are remarkably similar to differences seen by Cocks *et al.*[12] between two LES simulations on a 4 mm mesh that utilized different numerical solution methods. However, Cocks *et al.*[12] attributed their findings to differences in numerical dissipation and noise associated with the solution methods considered.

The significant differences in the predicted DES flow fields suggest the non-reacting bluff body case may allow for multiple vortex shedding modes in the numerical simulations. The shedding behaviour of the

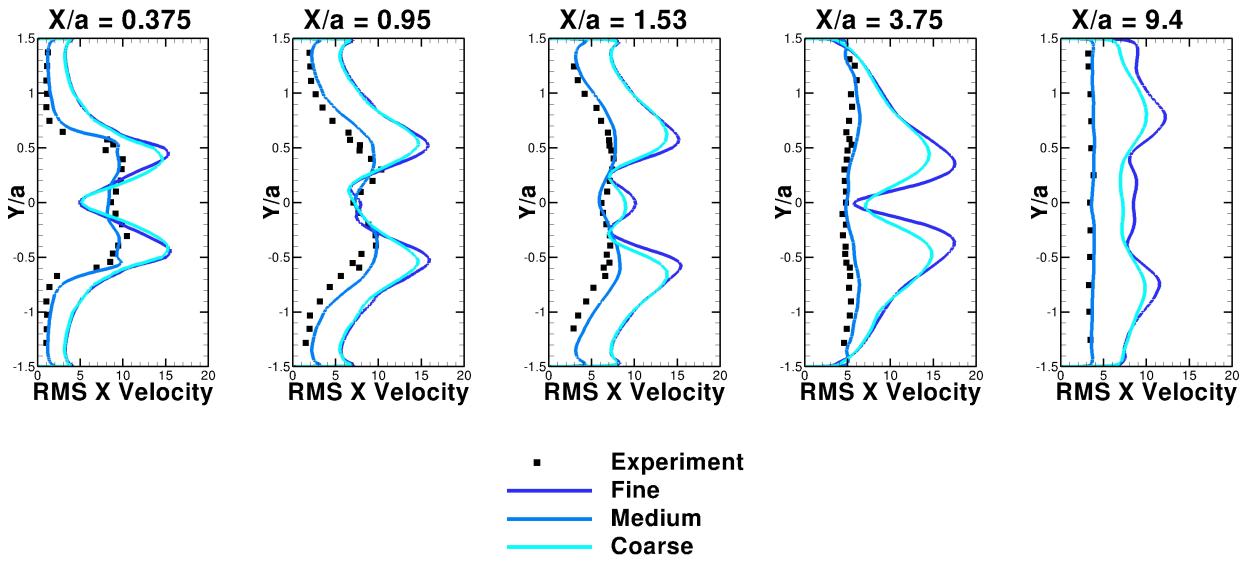

Figure 7. Non reacting bluff body flame stabilizer in duct flow initial mesh study RMS axial velocity (m/s) ($\tau_{ii}^{Modelled}$ included).

fine mesh predictions resemble the so-called low-speed mode as described by Zdravkovich,[29] where vortex production is driven by wake instabilities whereas, the shedding behaviour of the medium mesh predictions resemble the so-called high-speed mode as described by Zdravkovich,[29] where vortices develop in place on either side of the obstruction and are cut-off when they are strong enough to draw the shear layer from the opposite side across the wake. A rake of streak lines released on the downstream face of the obstruction as shown in Figures 9 and 10 re-enforce this hypothesis. In the fine mesh case, the streak lines coalesce and connect the vortices as would be expected if they were driven by a wake instability. In the medium mesh case, the streak lines in the wake are either consumed or reversed by the developing vortex, illustrating the cut-off mechanism in progress.

If the differences between these predictions are indeed a result of the vortex shedding mode, then it should be possible to establish both modes on the same mesh using the same simulation method. Therefore, using the coarse mesh and the DES method, four additional cases were run with varied pressure inlet settings and flow initialization as summarized in Table 2. These cases were simulated for $T = 0.15s \sim 2\,(L/U_{inlet})$ prior to collecting statistics and again for another $T = 0.15$ s in order to collect the necessary flow statistics. From this second set of simulation of the coarse mesh, it was readily established that both numerical solutions observed in the previous mesh study could be obtained on the coarse mesh by controlling the inlet total pressure and initializing the flow either with a constant axial velocity of 16.6 m/s or 0 m/s. The pressure inlet setting for the DES solutions with the vortex shedding mode that matched the experimental observations was obtained from the previous DES medium mesh solution and the pressure inlet setting for the DES calculations having the incorrect mode not matching the experiment was obtained from the previous DES fine mesh solution.

The predicted centerline axial velocity and pressure profiles of the DES method for these additional non-reacting flow cases on the coarse mesh are shown in Figure 12. As can be seen, case A follows the solution originally seen on the medium mesh while case D follows the solution originally found for the fine

Table 2. Inlet pressure boundary conditions and velocity field initialization used vortex mode study.

Case	Inlet Total Pressure (Pa)	Initialization Velocity (m/s)
A	334.3 (medium mesh inlet P_0)	16.6
B	334.3 (medium mesh inlet P_0)	0
C	517.3 (fine mesh inlet P_0)	16.6
D	517.3 (fine mesh inlet P_0)	0

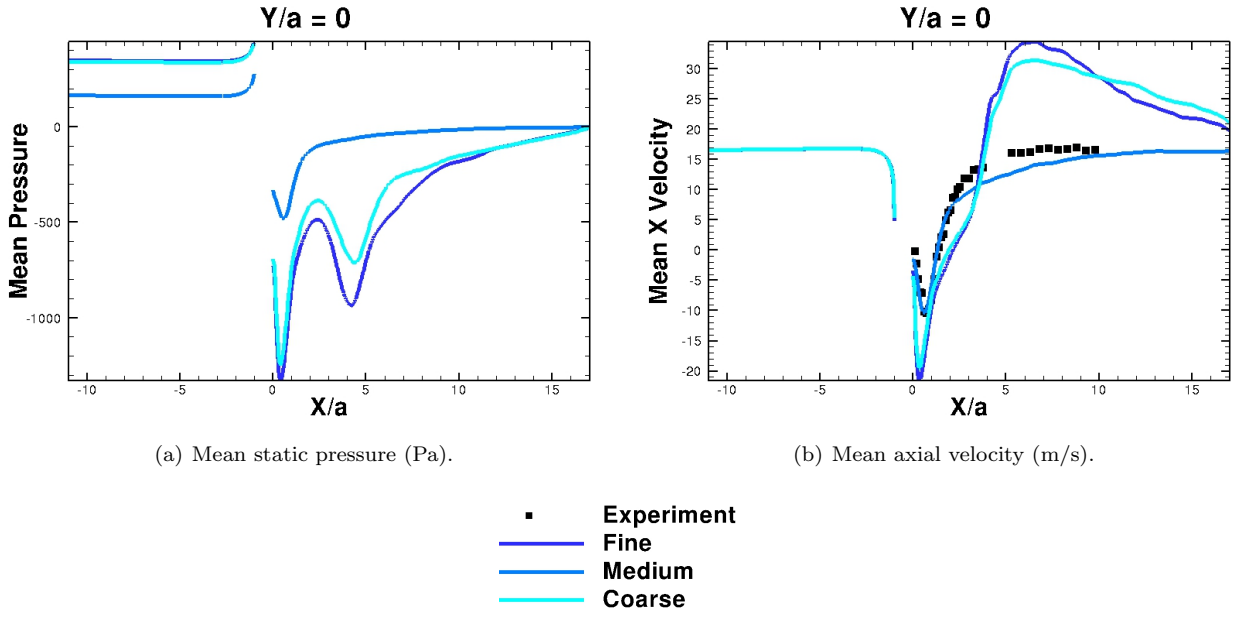

(a) Mean static pressure (Pa).

(b) Mean axial velocity (m/s).

Figure 8. Mesh study showing predicted mean centerline profiles of pressure and axial velocity for DES cases on the fine, medium, and coarse meshes.

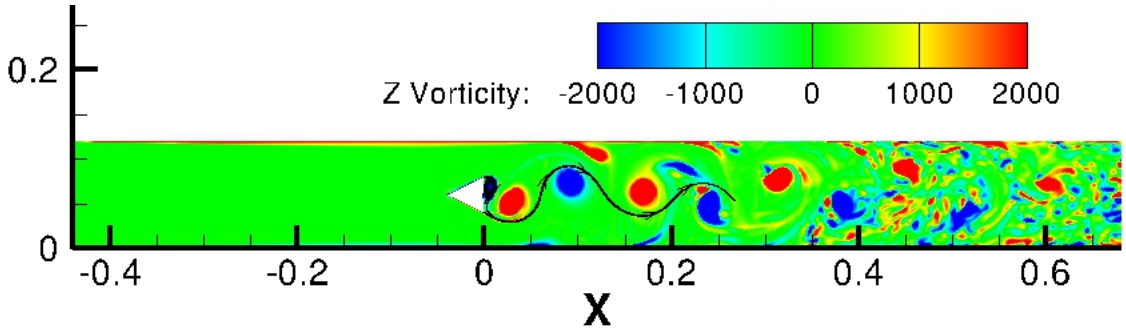

(a) Fine mesh.

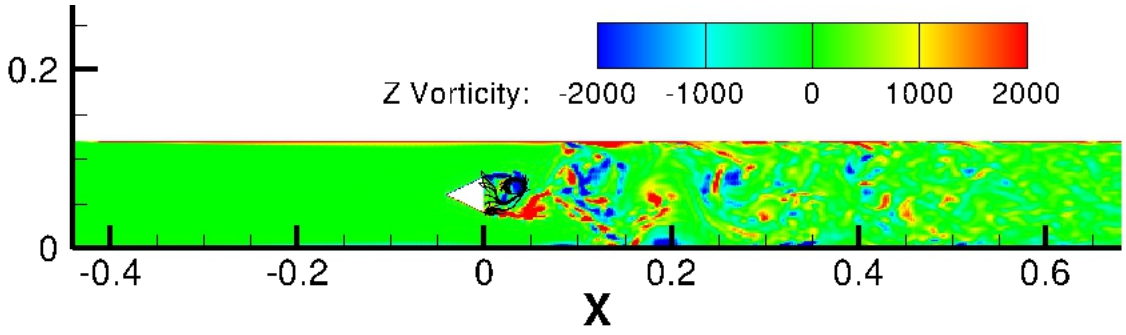

(b) Medium mesh.

Figure 9. Instantaneous Z vorticity contours (s^{-1}) with rake of streamtraces released from downstream face of the obstruction.

and coarse meshes. Despite being on the same mesh and having different pressure inlet settings, both cases A and D have roughly the same inlet velocities and also agree with the experimental inlet velocity. Case B appears to follow the solution of case D, but with a lower velocity as one would expect for the same flow case with a lower pressure difference. Case C follows the solution of case A but with a higher velocity as

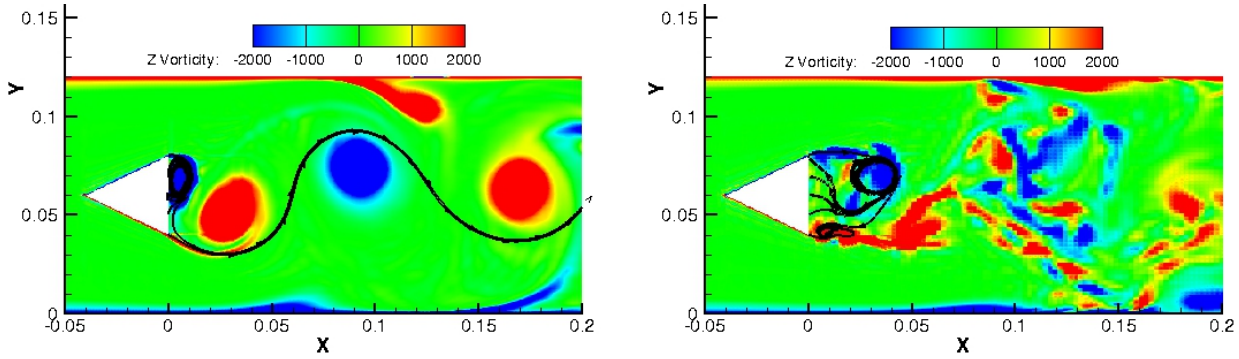

(a) Fine mesh.

(b) Medium mesh.

Figure 10. Instantaneous Z vorticity contours (s^{-1}) with rake of streak lines released from downstream face of the obstruction with close-up of streak lines.

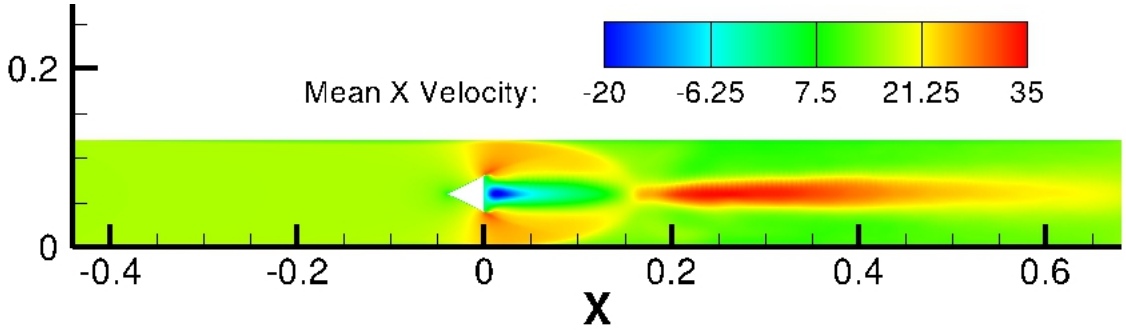

(a) Fine mesh.

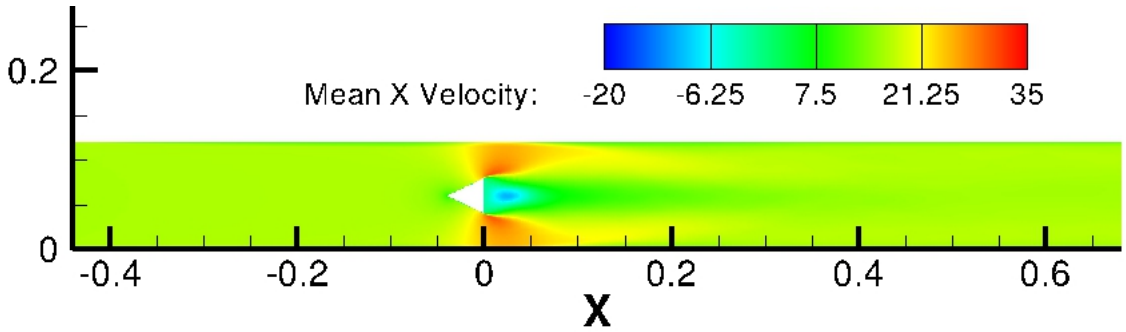

(b) Medium mesh.

Figure 11. Mean axial velocity contours (m/s).

one would expect for a higher pressure difference. This indicates that the initial conditions may also be key to obtaining the correct solution corresponding to the experiment. However, given that both case A and case D have inlet velocities which agree with the experimental inlet velocity despite being representative of different modes, it is clear that a velocity inlet boundary condition would be ambiguous between the two modes. This ambiguity was observed in the previous DES results of the mesh study, where both modes were observed despite all meshes having the same velocity inlet boundary conditions.

The mesh study on the fine, medium, and coarse meshes was then repeated with a pressure inlet set to a total pressure of 334.3 Pa and the flow initialized at a constant axial velocity of 16.6 m/s. These simulations were performed for a time period of $T = 0.15s \sim 2\,(L/U_{inlet})$ prior to collecting statistics and for an additional time of $T = 0.15s \sim 2\,(L/U_{inlet})$ to collect flow statistics. The results for the mean and RMS of the axial velocity component for this second set of simulations on the mesh with successively increasing resolution are shown in Figures 13 and 14. It is clear that the DES results on all three meshes now all agree,

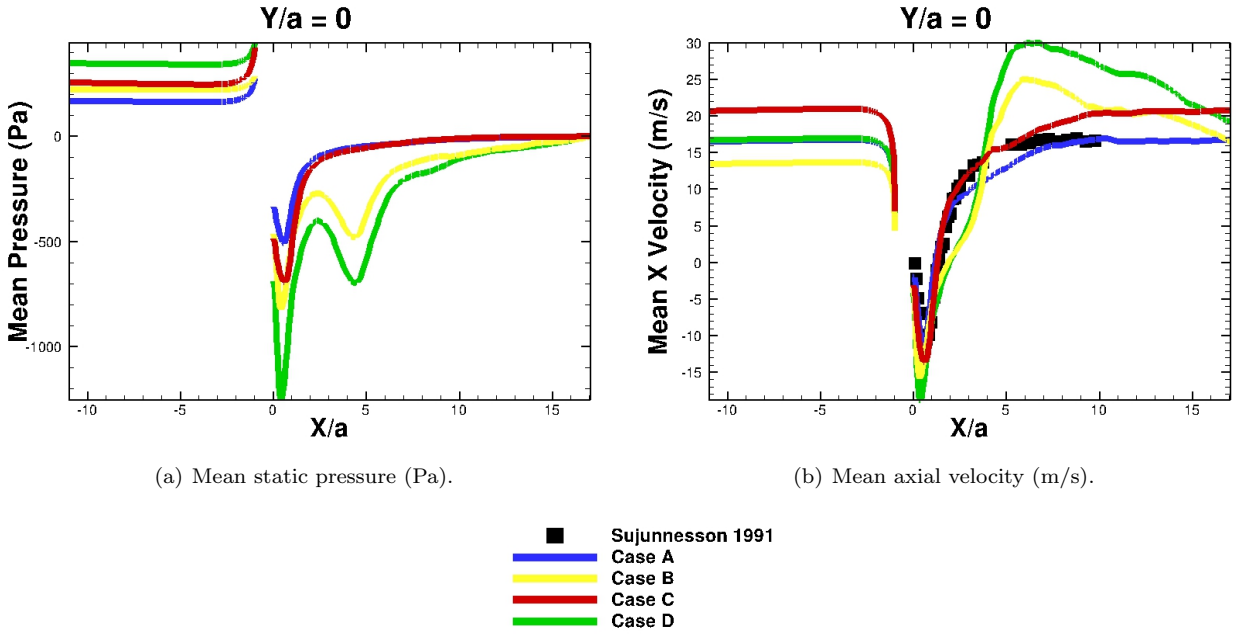

(a) Mean static pressure (Pa).

(b) Mean axial velocity (m/s).

Figure 12. Boundary data study showing predicted mean centerline profiles of pressure and axial velocity for DES cases A, B, C, and D.

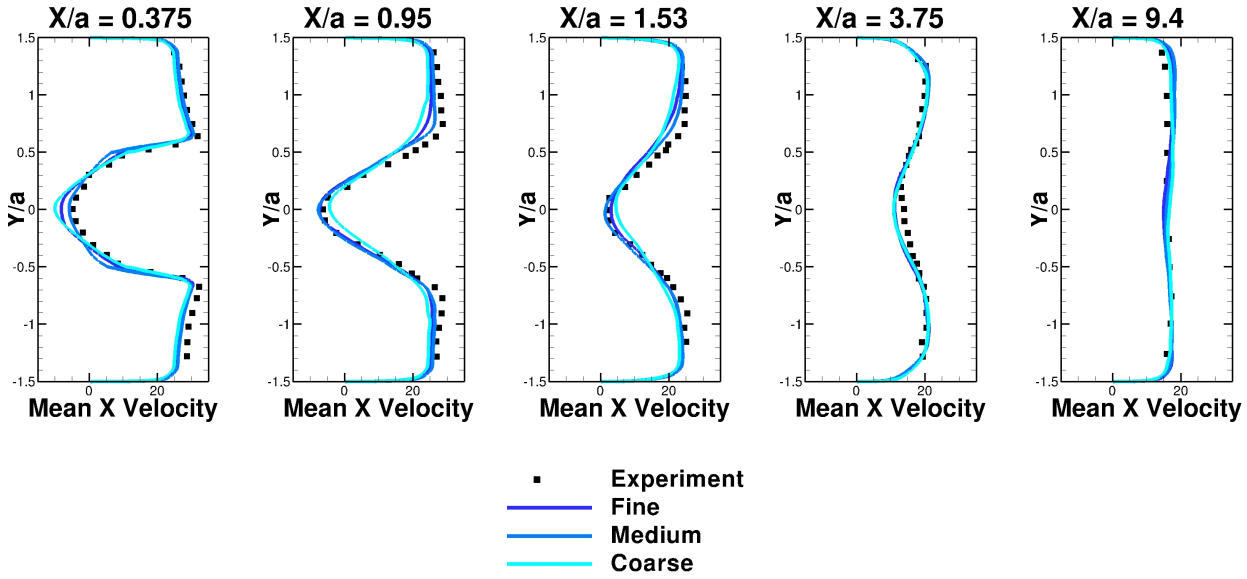

Figure 13. Bluff body flame stabilizer in duct flow second mesh study mean axial velocity (m/s).

i.e., are associated with the same vortex shedding mode. Moreover, the DES predictions of the mean axial and RMS velocity profiles downstream of the bluff body agree very well with the experimental data for all three meshes.

The issues with initial and boundary prescription described in this section are not unique to DES and would be common to all LES like methods. The findings serve as a reminder that transient simulations can be quite challenging and that phenomenon, such as multiple solution modes, are possible.

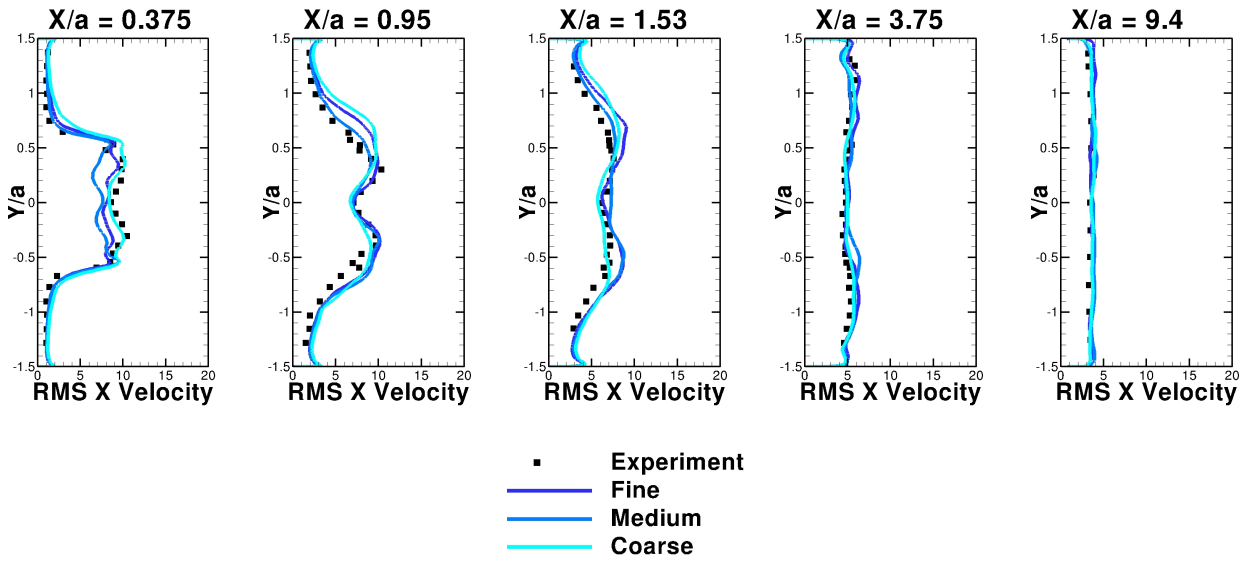

Figure 14. Bluff body in flame stabilizer second mesh study RMS axial velocity (m/s) ($\tau_{ii}^{Modelled}$ included).

VI.B. Comparison with Alternative Turbulence Treatments

In addition to a DES simulation, laminar, URANS, LES, and DLES simulations were conducted on the coarse mesh for the non-reactive flow case. A pressure inlet was utilized instead of a velocity inlet due to the possibility of multiple unsteady modes related to vortex shedding as discussed previously in Section VI.A. The mean and RMS velocity results are shown in Figures 15 and 16, respectively.

As can be seen in Figures 15 and 16, the predictions of DES, LES, and DLES all compare well with experimental results while URANS predictions do not. Interestingly, the predictions of the laminar simulation also seem to agree surprisingly well with the other methods and experimental data. This suggests that the flow is dominated by the large scale vortex structures and is relatively insensitive to treatments for the sub-grid turbulence. The poor performance of URANS, particularly in comparison to the laminar simulations, suggests that URANS is incorrectly predicting the large scale vortices to be representative of a complete turbulence spectrum at scales far smaller than them, which is likely not the case. This viewpoint is also supported by the large peaks in the RMS velocity values predicted by URANS, as seen in Figure 16.

Additionally, for the DES method, the ratio of modelled turbulent kinetic energy to total turbulent kinetic energy was investigated and shown in Figure 17. Where the total turbulent kinetic energy, k_{total}, is defined as the time averaged value of the resolved turbulent kinetic energy, $k_{resolved}$, plus the time averaged modelled turbulent kinetic energy, $k_{modelled}$. The intended LES region for this stabilizer flow field was the region downstream of the obstruction. As can be seen, the modelled turbulent kinetic energy is estimated to be less than 20% of the total turbulent kinetic energy in this intended LES region. The simulation therefore meets the recommended maximum ratio between $k_{modelled}$ and $k_{resolved}$ as suggested by Pope.[30]

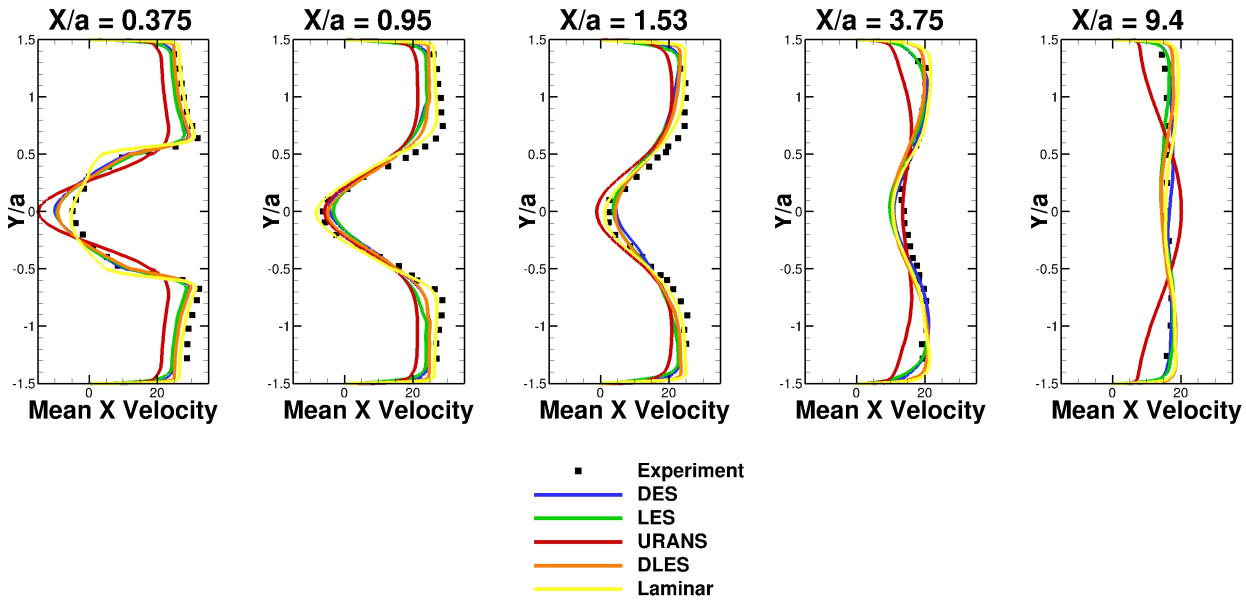

Figure 15. Bluff body flame stabilizer in duct flow coarse mesh mean velocity comparisons (m/s).

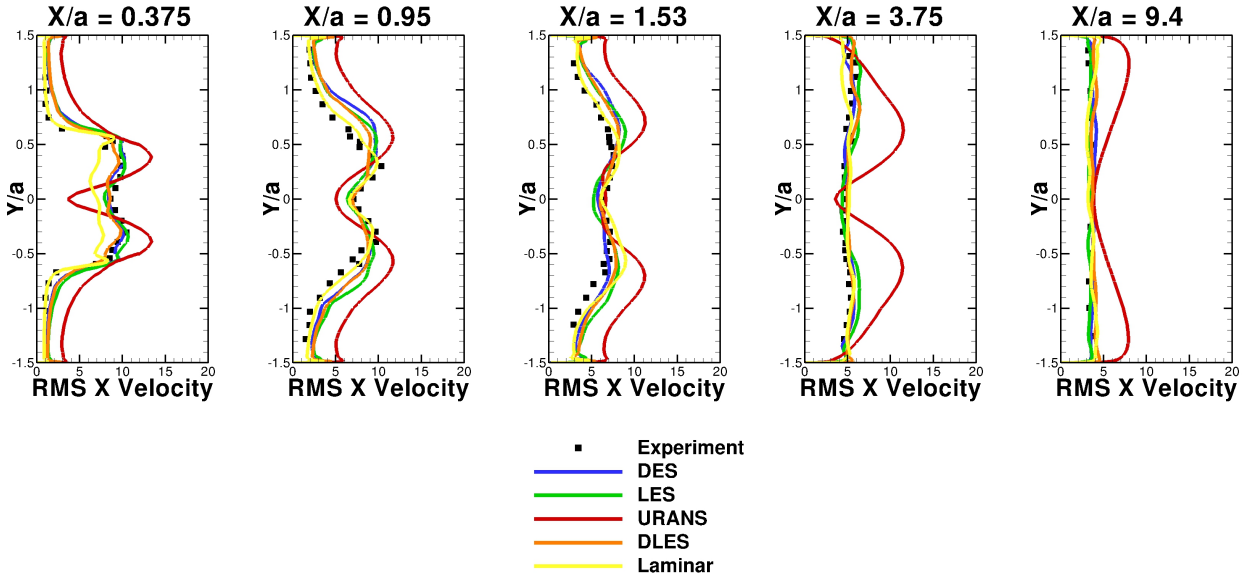

Figure 16. Bluff body flame stabilizer in duct flow coarse mesh RMS velocity comparisons ($\tau_{ii}^{Modelled}$ included) (m/s).

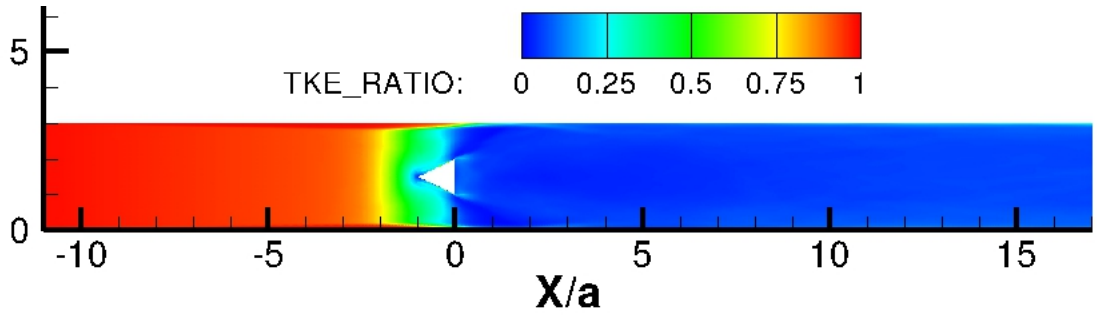

Figure 17. Ratio of $k_{modelled}$ to k_{total} for bluff body flame stabilizer in duct flow DES simulation on coarse mesh.

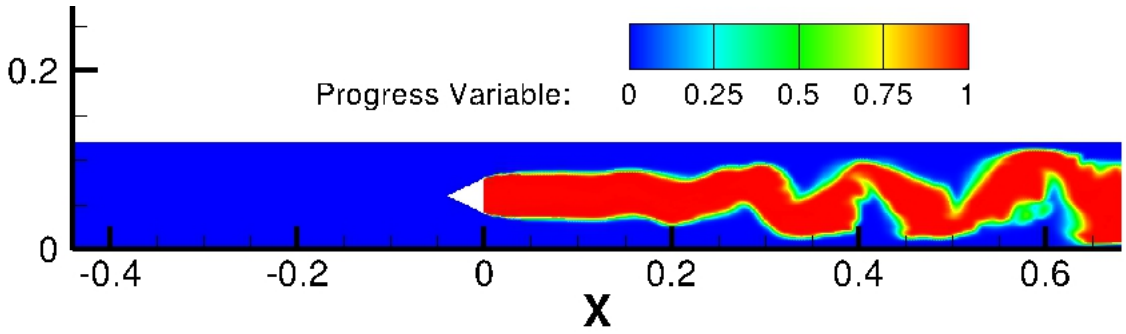

(a) Coarse mesh.

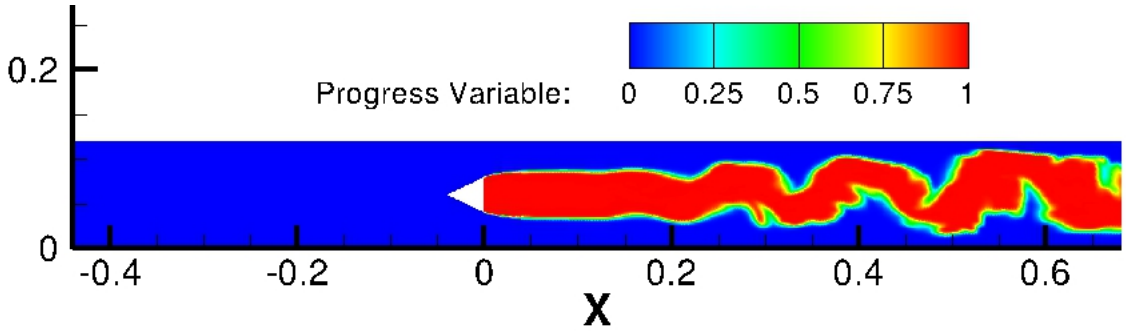

(b) Medium mesh.

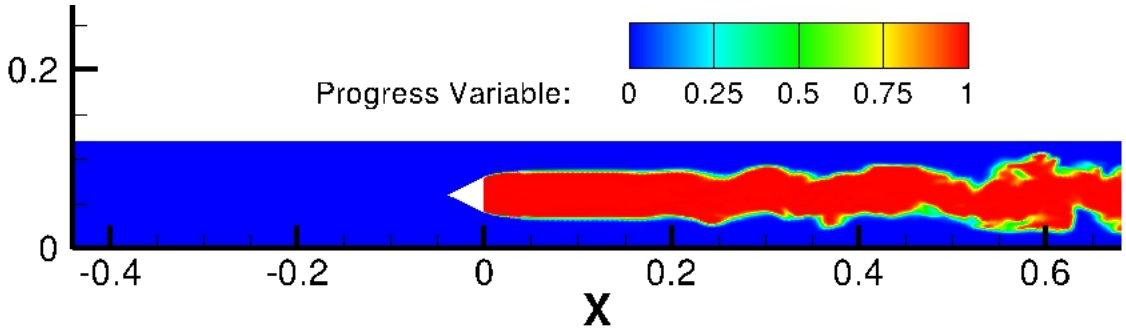

(c) Fine mesh.

Figure 18. Instantaneous combustion progress variable contours on coarse, medium, and fine meshes.

VII. DES Results and Discussion for Reactive Flow Field

Although different possible vortex shedding modes played a role in the non-reacting case, this was not observed in the present simulations for the reactive flow field. As discussed in Sjunneesson *et al.*[10], the non-reacting case displayed very strong vortex shedding which was not present in the reacting case. As such, the reacting flow simulations were conducted herein using a mass flow inlet boundary condition that corresponded to the experimental bulk velocity of 17.3 m/s. The reactive flow simulations were then conduced on meshes corresponding to all three mesh resolutions (i.e., on the coarse, medium, and fine meshes as described previously) and their predictions were compared to the available experimental results.

Predictions of the instantaneous values for the progress variable the mean centerline axial velocity component and fluctuation intensity obtained using the coarse, medium, and fine meshes for the reactive case are shown in Figures 18 and 19, respectively. Unfortunately, some of the important features of the flame structure observed in the experiments were not predicted by the DES simulations on any of the three meshes, such as the shear layer roll-up. As can be seen in the predicted instantaneous progress variable contours on each mesh in Figure 18, the flame does not display significant unsteady behaviour until well past the obstruction. In fact, the unsteady features of the flame would appear to occur further downstream on the

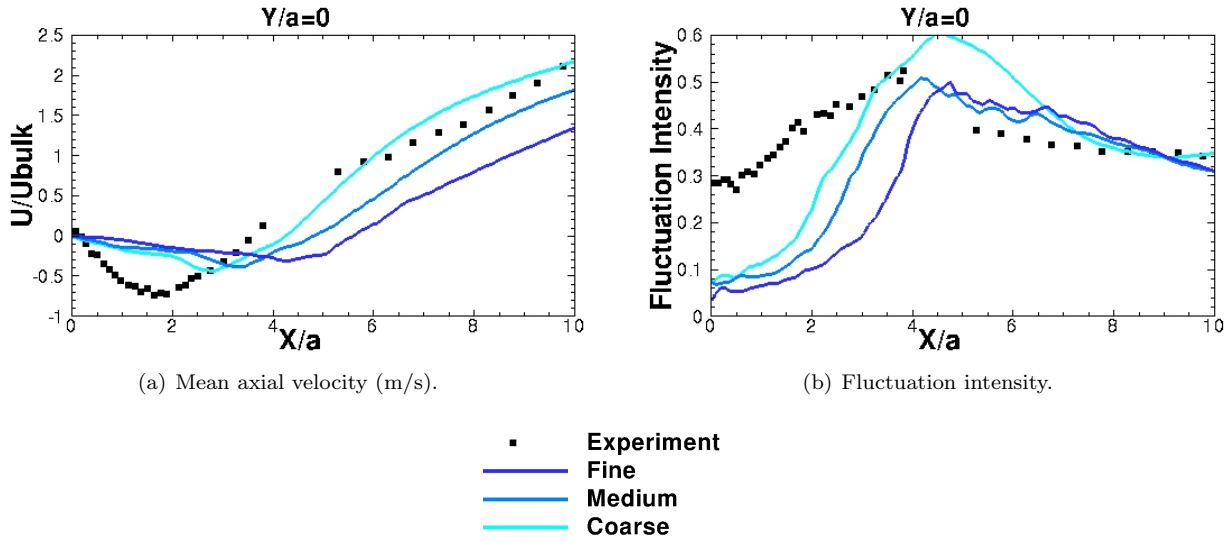

(a) Mean axial velocity (m/s).

(b) Fluctuation intensity.

Figure 19. Predicted mean centerline profiles of axial velocity component and fluctuation intensity for premixed combustion mesh study.

fine mesh than for the result corresponding to the coarse mesh. In Figure 19, which shows the centerline axial velocity and fluctuation intensity, it can be seen that the flame remains steady farther downstream on finer meshes than on coarse meshes. It is speculated that the failure of DES to predict these salient features of the bluff-body stabilizer flow for the reactive case is partially due to the rather simple flamelet-based combustion model as described in Section IV. Additionally, the current choice of the critical flame strain rate so as to prevent local extinction of the flame may also be hampering the accuracy of the predictions. Without this modelling for the effects of flame stretch, the combustion model predictions are relatively insensitive to the high strain rate experienced in the shear layers. This would suggest that improved results may be possible through a judicious choice of the critical strain rate and an examination of this parameter on the simulation results would seem warranted but was beyond the scope of the present study.

Mean axial velocity, axial RMS velocity, and mean temperature were also compared as shown in Figures 20, 21, and 22, respectively. Despite the somewhat unimpressive results for the instantaneous flow of the reactive flow field described above, relatively good agreement can be observed between the predicted mean axial velocity profiles and experiment at the various stations up to $X/a = 3.75$. Further downstream of this station, the predicted results on the various meshes do not appear to be in good agreement with each other (indicating issues with mesh convergence and the need for a finer mesh) or the experiments. Similar findings are suggested by the predictions of the mean temperature profiles across the duct downstream of the stabilizer. Conversely, while the predictions of the profiles of the RMS of the axial velocity component on the three meshes are in relative agreement with each other, they underpredicted and do not agree well with the experimental results for much of the downstream region of the stabilizer up to station $X/a = 3.75$, supporting the observation that the unsteady features of the flame are not well resolved. It should be emphasized that this relative lack of grid convergence and agreement with experiment for the reactive case would seem in rather stark contrast to the generally good agreement between the DES predictions and experiment that was obtained on all three meshes for the non-reacting case.

VIII. Conclusions

For the non-reacting DES simulations of the bluff body flame stabilizer in duct flow of Sjunnesson *et al.*,[10] it was determined that two different vortex shedding modes are possible in the numerical solutions, depending on initial conditions and boundary conditions. Both of these modes can be realized on the same mesh by utilizing the DES model. Without consideration of these different modes, simulation agreement with experimental results may in many cases seem somewhat random. Additionally, the DES method is shown to be in LES mode downstream of the bluff body and the modelled stresses for this case were small even on relatively coarse meshes, suggesting the flow is dominated by the large scale vortices generated by

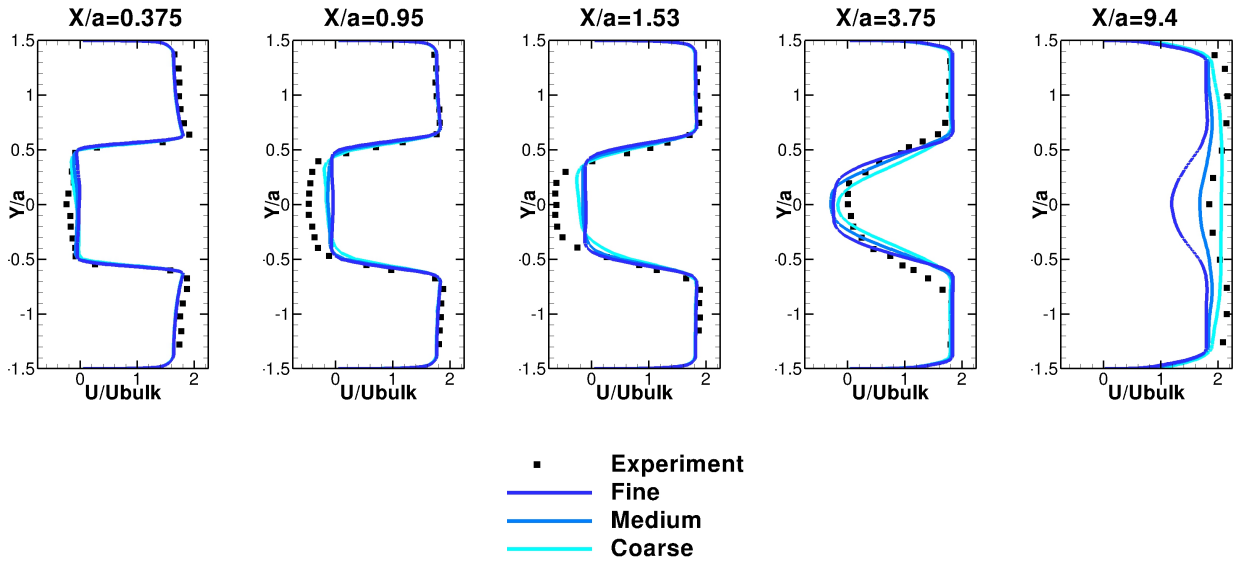

Figure 20. Bluff body flame stabilizer premixed combustion in duct flow mesh study mean axial velocity (m/s).

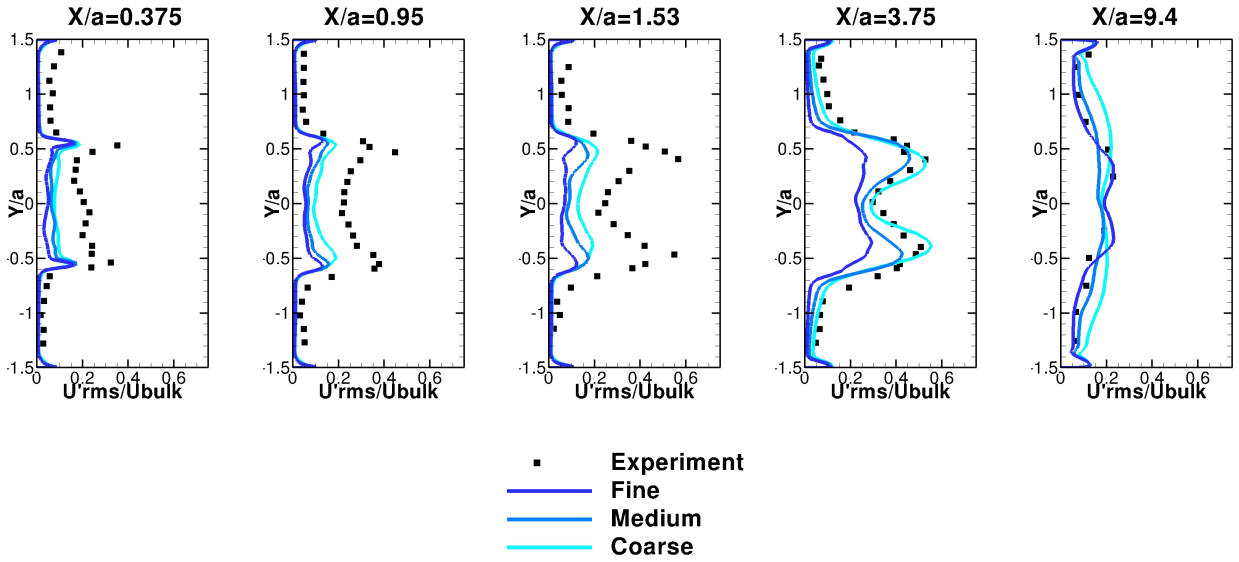

Figure 21. Bluff body flame stabilizer premixed combustion in duct flow mesh study RMS axial velocity (m/s) ($\tau_{ii}^{Modelled}$ included).

the obstruction. As such, good agreement between the predicted DES simulations and experimental data were observed for the non-reacting case on all three meshes considered herein (coarse, medium, and fine meshes) suggesting some level of confidence in the resolution for at least the fine mesh.

In contrast, DES simulations of the reactive flow field using a simple premixed flamelet-based combustion model failed to predict several of the important and dominate unsteady features and structures of the flame downstream of the stabilizer, despite the fact that the mean velocity field appeared to be rather well predicted. Additionally, the DES results on the successively refined meshes suggested a dependence of the current results on grid resolution. Further tuning of the flame stretch model in the flamelet-based combustion model and the use of finer meshes may offer avenues for improved predictions of this reactive flow and will be the subject of future follow-on studies.

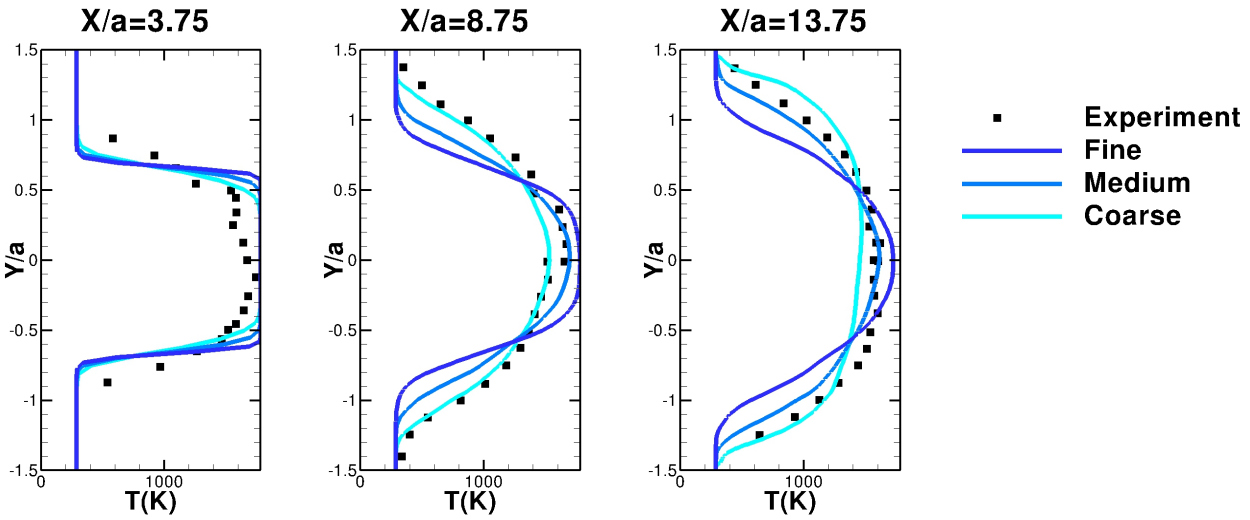

Figure 22. Bluff body flame stabilizer premixed combustion in duct flow mesh study mean temperature (K).

Acknowledgements

All of the computations were performed on the GPC supercomputer at the SciNet HPC Consortium. SciNet is funded by: the Canada Foundation for Innovation under the auspices of Compute Canada; the Government of Ontario; Ontario Research Fund - Research Excellence; and the University of Toronto. Financial support for this project was primarily provided by Pratt & Whitney Canada and NSERC through their Industrial Research Chair in Aviation Gas Turbine Combustion/Emissions Research and Design System Optimization program. Additional financial support was provided by the International Society of Transport Aircraft Trading through their scholarship program.

References

[1]Fröhlich, J. and von Terzi, D., "Hybrid LES/RANS Methods for the Simulation of Turbulent Flows," *Progress in Aerospace Sciences*, Vol. 44, No. 5, 2008, pp. 349–377.

[2]Spalart, P., Jou, W., Strelets, M., and Allmaras, S., "Comments on the Feasibility of LES for Wings, and on a Hybrid RANS/LES Approach," *Advances in DNS/LES*, Vol. 1, 1997, pp. 4–8.

[3]Spalart, P., Deck, S., Shur, M., and Squires, K., "A New Version of Detached-Eddy Simulation, Resistant to Ambiguous Grid Densities," *Theoretical and Computational Fluid Dynamics*, Vol. 20, No. 3, 2006, pp. 181–195.

[4]Travin, A., Shur, M., Strelets, M., and Spalart, P., "Physical and Numerical Upgrades in the Detached-Eddy Simulation of Complex Turbulent Flows," *Advances in LES of Complex Flows*, edited by R. Friedrich and W. Rodi, Springer Netherlands, 2000, pp. 239–254.

[5]Spalart, P., "Detached-Eddy Simulation," *Annual Review of Fluid Mechanics*, Vol. 41, 2009, pp. 181–202.

[6]Choi, J., Yang, V., Ma, F., and Jeung, I., "Detached Eddy Simulation of Combustion Dynamics in Scramjet Combustors," *Joint Propulsion Conference and Exhibit*, 43, AIAA/ASME/SAE/ASEE, 2007.

[7]Sainte-Rose, B., Bertier, N., Deck, S., and Dupoirieux, F., "Delayed Detached Eddy Simulation of a Premixed Methane Air Flame Behind a Backward Facing Step," *Joint Propulsion Conference and Exhibit*, 44, AIAA/ASME/SAE/ASEE, 2008.

[8]Sainte-Rose, B., Bertier, N., Deck, S., and Dupoirieux, F., "A DES Method Applied to a Backward Facing Step Reactive Flow," *Comptes Rendus Mcanique*, Vol. 337, No. 6-7, 2009, pp. 340–351.

[9]Menter, F., Kuntz, M., and Langtry, R., "Ten Years Industrial Experience with the SST Turbulence Model," *In Turbulence, Heat and Mass Transfer*, edited by K. Hanjalić, Y. Nagano, and M. Tummers, Begell House, Inc., 4th ed., 2003, pp. 625–632.

[10]Sjunnesson, A., Nelsson, C., and Max, E., "LDA Measurements of Velocities and Turbulence in a Bluff Body Stabilized Flame," *Laser Anemometry*, Vol. 3, 1991, pp. 83–90.

[11]Sjunnesson, A. and Henrikson, P., "CARS Measurements and Visualization of Reacting Flows in a Bluff Body Stabilized Flame," *28th AIAA Joint Propulsion Conference and Exhibit Nashville TX, July*, 1992.

[12]Cocks, P., Sankaran, V., and Soteriou, M., "Is LES of Reacting Flows Predictive? Part 1: Impact of Numerics," *51st AIAA Aerospace Sciences Meeting, Grapevine TX, January*, 2013.

[13]Porumbel, I. and Menon, S., "Large Eddy Simulation of Bluff Body Stabilized Premixed Flame," *AIAA Paper*, , No. 2006-152, 2006.

[14]Fureby, C., "Large Eddy Simulation of Combustion Instabilities in a Jet Engine Afterburner Model," *Combustion science and technology*, Vol. 161, No. 1, 2000, pp. 213–243.

[15]Fureby, C., "On Subgrid Scale Modeling in Large Eddy Simulations of Compressible Fluid Flow," *Physics of Fluids*, Vol. 8, No. 5, 1996, pp. 1301–1311.

[16]Menter, F. and Egorov, Y., "The Scale-Adaptive Simulation Method for Unsteady Turbulent Flow Predictions. Part 1: Theory and Model Description," *Flow, Turbulence and Combustion*, Vol. 85, No. 1, 2010, pp. 113–138.

[17]Hasse, C., Sohm, V., Wetzel, M., and Durst, B., "Hybrid URANS/LES Turbulence Simulation of Vortex Shedding Behind a Triangular Flameholder," *Flow, Turbulence and Combustion*, Vol. 83, No. 1, 2009, pp. 1–20.

[18]Comer, A., Huang, C., Rankin, A., Harvazinski, M., and Sankaran, V., "Modeling and Simulation of Bluff Body Stabilized Turbulent Premixed Flames," *54th AIAA Aerospace Sciences Meeting*, 2016.

[19]Sardeshmukh, S., Huang, C., and Anderson, W., "Impact of Chemical Kinetics on the Predictions of Bluff Body Stabilized Flames," 2016.

[20]"Model Validation for Propulsion Workshop," http://mvpws.stanford.edu/.

[21]Piomelli, U., "Large-Eddy Simulation: Achievements and Challenges," *Progress in Aerospace Sciences*, Vol. 35, 1999, pp. 335–362.

[22]Germano, P., Piomelli, U., Moin, P., and Cabot, W., "A Dynamic Subgrid-Scale Eddy Viscosity Model," *Physics of Fluids*, Vol. 3, No. 7, 1991, pp. 1760–1765.

[23]Patankar, S. and Spalding, S., "A Calculation Procedure for Heat, Mass and Momentum Transfer in Three-Dimensional Parabolic Flows," *International Journal of Heat and Mass Transfer*, Vol. 15, 1972, pp. 1787–1806.

[24]Barth, T. and Jespersen, D., "The Design and Application of Upwind Schemes on Unstructured Meshes," *Aerospace Sciences Meeting*, No. AIAA-89-0366 in 27, AIAA, 1989.

[25]Poinsot, T. and Veynante, D., *Theoretical and Numerical Combustion*, RT Edwards, Inc., 2005.

[26]Bray, K., "Turbulent Flows With Premixed Reactants," *Turbulent Reacting Flows*, Springer, 1980, pp. 115–183.

[27]Zimont, V., Polifke, W., Bettelini, M., and Weisenstein, W., "An Efficient Computational Model for Premixed Turbulent Combustion at High Reynolds Numbers Based on a Turbulent Flame Speed Closure," *ASME 1997 International Gas Turbine and Aeroengine Congress and Exhibition*, American Society of Mechanical Engineers, 1997, pp. V002T06A054–V002T06A054.

[28]Spalart, P., "Young-Person's Guide to Detached-Eddy Simulation Grids," Contractor Report NASA/CR-2001-211032, NASA, 2001.

[29]Zdravkovich, M., "Different Modes of Vortex Shedding: An Overview," *Journal of fluids and Structures*, Vol. 10, No. 5, 1996, pp. 427–437.

[30]Pope, S., *Turbulent Flows*, Cambridge University Press, 2000.